Development and validation of a CT-TA nomogram for preoperatively differentiating thymic epithelial tumor histologic subtypes

Caiyue Ren (rencaiyue@163.com)
Shanghai Proton and Heavy Ion Center
Mingli Li
Shanghai Proton and Heavy Ion Center
Yunyan Zhang
Shanghai Proton and Heavy Ion Center
Shengjian Zhang
Fudan University Shanghai Cancer Center

Research

Keywords: thymic epithelial tumor, classification, nomogram, computed tomography, texture analysis

Posted Date: February 24th, 2020

DOI: https://doi.org/10.21203/rs.2.24242/v1

Abstract

Background: Thymic epithelial tumors (TETs) are the most common primary tumors in the anterior mediastinum with considerable histologic heterogeneity. This study aimed to develop and validate a nomogram based on computed tomography (CT) and texture analysis (TA) for preoperatively predicting pathological classification for TET patients.

Methods: Totally 172 patients with pathologically confirmed TET after surgery were retrospectively analyzed and randomly divided into a training cohort (n=120) and a validation cohort (n=52). Preoperative clinical demographic, CT signs and texture features of each patient were analyzed and prediction models were developed using the least absolute shrinkage and selection operator (LASSO) regression. The performance of models was evaluated and compared by the area under receiver operating characteristic (ROC) curve (AUC) and DeLong test. The clinical application value of models was determined through the decision curve analysis (DCA). Then a nomogram was developed based on the model with the best predictive accuracy and clinical utility and validated using the calibration plots.

Results: Totally 87 patients with low-risk TET (LTET) (types A, AB, B1) and 85 patients with high-risk TET (HTET) (types B2, B3, C) were enrolled in this study. We separately constructed 4 prediction models for differentiating LTET from HTET using clinical, CT, texture features and their combination. These 4 prediction models achieved AUC values of 0.66, 0.79, 0.82, 0.88 in the training cohort and 0.64, 0.82, 0.86, 0.94 in the validation cohort, respectively. DeLong test and DCA analysis showed that the Combined model consisting of 2 CT signs and 2 texture parameters held the highest predictive efficiency and clinical utility ($p < 0.05$). A prediction nomogram was subsequently developed using the combined model's 4 independently risk factors. The calibration curves indicated a good consistency between the actual observation and nomogram prediction for differentiating TET classifications.

Conclusion: A prediction nomogram incorporating both the CT and texture parameters was constructed and validated in our study, which was conveniently used to facilitate the preoperative individualized prediction of simplified histologic subtypes in TET patients, assisting in clinical treatment decision making and achieving precision treatment.

Background

Thymic epithelial tumors (TETs), which are the most common primary tumors in the anterior mediastinum, are well-known for heterogeneity in the oncologic and biologic behaviors [1]. According to the morphology of epithelial cells as well as the lymphocyte-to-epithelial cell ratio, the World Health Organization (WHO) classification which was proposed in 2015 classified TETs into six subtypes (thymoma: types A, AB, B1, B2 and B3; thymic carcinoma: type C), which is recognized as the basis of the clinical treatment decision making and an independent prognostic factor in TETs [2–4]. Previous studies have shown that the invasiveness of each subtype increased in turn, and patients in low-risk TET (LTET) (types A, AB, B1) usually had more chances to be completely resected, lower tumor recurrence rate and

higher survival rate than ones in high-risk TET (HTET) (types B2, B3, C) [5–7]. Moreover, HTET patients can benefit more from adjuvant treatment than LTET patients [8]. Thus, preoperative knowledge of histologic classification can provide valuable information for treatment decision making and prognostic evaluation in TET patients.

Currently, at least 3 imaging modalities are used for TET patients. Although positron emission tomography-computed tomography (PET/CT) is the most sensitive and accurate method for tumors [9], it is not recommended as a routine examination because of the high cost and great radiation damage [10]. Magnetic resonance imaging (MRI) may be another method that could provide functional quantitative indicators for TETs [11], but it is not appropriate for patients with mental implants or poor respiratory control. Computed tomography (CT) is widely recognized as the main imaging method for the diagnosis, differentiation and evaluation of curative effect in TET patients due to its convenient operation, good image quality, moderate price and less contraindications [12]. The signs on CT images, such as size, location of the lesions, as well as the presence of pericardium or pleural effusion and distant metastases, are helpful to preliminarily judge the invasiveness of TETs [13–15]. However, they are of limited value for further accurate assessment tumor heterogeneity or differentiation of its histological subtypes [16].

Texture analysis (TA) based on conventional medical images has been used to quantity assessment of tumor heterogeneity by analyzing the distribution and relationship of pixel or voxel gray levels in the lesion area [17; 18]. Previous studies have revealed that TA, as a non-invasive imaging tool, has great potential in predicting pathologic features, response to therapy and prognosis of head and neck cancer, rectal cancer, et.al [19; 20]. Moreover, CT quantitative TA has been conducted for preoperative assessment of TETs and shown good diagnostic performance in differentiating tumor types and stages [21; 22]. However, only texture parameters extracted from CT images were analyzed in above studies, whether the prediction model combines with CT signs and texture parameters can further improve the discrimination performance is an interesting problem that requires investigation.

Hence, the aim of this study was to develop and validate a nomogram consisting of CT morphological features and texture parameters for differentiating the simplified histologic subtypes in patients with TETs.

Methods

Patients

We conducted a retrospective analysis of patient records with TETs diagnosed between January 2011 to April 2019 at two cancer centers: Shanghai Proton and Heavy Ion Center (institution A) and Fudan University Shanghai Cancer Center (institution B). This study was approved by the ethics committees of these two institutions and the requirement for informed consent was waived. The inclusion criteria including the following: 1) underwent standard contrast-enhanced CT at above two institutions less than 14 days before surgery; 2) patients who underwent surgery at institution B for TETs with curative intent; 3) information of postoperative pathologically confirmed TETs histologic subtypes available. The

exclusion criteria including the following: 1) previous history of TETs or other cancer; 2) preoperative therapy (radiotherapy, chemotherapy or chemoradiotherapy); 3) poor image quality affects lesion segmentation.

Finally a total of 172 patients were enrolled and analyzed (95 males and 77 females; mean age, 54.56±10.67 years; range, 24-77 years). The WHO histologic classification of TETs were confirmed by reviewing the surgical findings and pathological examinations from the electronic medical record system of institution B.

Patients were divided into a training cohort (n=120) and a validation cohort (n=52) after simple randomization at a ratio of 7 to 3. Baseline data pertaining to demographics of each patient, including gender, age, symptom was reviewed and recorded.

CT images acquisition and analysis

Patients generally underwent contrast-enhanced CT of the entire thorax according to standard clinical scanning protocols (120 kV, 200 mA, slice thickness and interval of 1.0 mm) on the 32- or 64-slice Siemens Sensation system (Siemens Medical System, Forchheim, Germany). Patients were in a supine position, and the scan range included all lesion areas. After the plain CT, a total of 80-120 mL (1.5 mL/kg) of iodinated contrast material (Ultravist 370, Bayer Schering Pharma, Berlin, Germany) was injected with a pump injector (Ulrich CT Plus 150, Ulrich Medical, Ulm, Germany) at a flow rate of 3 mL/s into the antecubital vein. The enhanced scans started 35 seconds after the contrast media reached 100 Hu. The images were uploaded to picture archiving and communication system (PACS) (Carestream, Ontario, Canada) workstations for image segmentation and analysis.

Two radiologists (reader 1: CY.R, with 3 years of experience in CT diagnosis, now working in the department of Nuclear Medicine; reader 2: YY.Z, a radiologist who has 14-years working experience) assessed the following morphological features of each lesion without knowing the exact pathologic subtypes of TETs by consensus: tumor size (the longest diameter measured by the largest cross section of the mass and the shortest diameter perpendicular to it), location (unilateral or cross midline), shape (regular or irregular), boundary (smooth or rough), density (the presence of calcification, cystic necrosis), the degree of enhancement (mild, moderate or obvious enhancement), mediastinal fat line (clear, unclear), pericardium or pleural effusion and metastasis (present or absent).

Tumor segmentation and texture feature extraction

Tumor segmentation and feature extraction were performed using the LIFEx (version 5.10, CEA-SHFJ, Orsay, France) package. The above two radiologists selected the largest slice of the tumor at three-dimensional (3D) images to delineate the region of interest (ROI) by consensus (**Fig. 1 a-d**). The ROI selection should include all tumors and avoid blood vessels, calcification and gas.

A total of 43 texture features were extracted automatically [23], including 2 shape features, 9 first-order histogram features, 7 Gray-Level Co-occurrence Matrix (GLCM) features, 11 Gray-Level Run Length Matrix

(GLRLM) features, 3 Neighboring Gray-Level Dependence Matrix (NGLDM) features and 11 Gray-Level Zone Length Matrix (GLZLM) features. The details of texture features were described in supplementary data.

Statistical analysis

Statistical analysis was performed in R (version 3.6.0, http://www. r-project. org). A two-tailed *p* value of < 0.05 was used as the criterion to indicate a statistically significant difference. The Mann-Whitney *U* test was used to assess differences in continuous variables, whereas the $\chi 2$ test was used for categorical variables. Intra- and interclass correlation coefficients (ICCs) were used to evaluate the consistency and reproducibility of the intra- and inter-observer agreement of extracting features by two-level radiologists. An ICC greater than 0.75 indicated good consistency.

Feature selection and prediction model establishment

Univariate analysis was applied to the clinical, CT and texture features to identify the most relevant predictors of the type of TETs using Pearson's correlation test in the training cohort. Multivariate analysis was performed by least absolute shrinkage and selection operator (LASSO) regression with 10-folds cross validation which was used to select the most useful features [24; 25]. The prediction models which performed to differentiating LTET from HTET were developed by the linear fusion of selected features weighted by their coefficients, with prediction scores (Pre-scores) of each model calculated for each patient.

Prediction performance and Clinical utility of predictive models

The performance of the models was evaluated by the area under the receiver operating characteristic (ROC) curve (AUC) and compared by Delong test. The AUCs, sensitivity, specificity and accuracy with 95 % confidence intervals (CIs) were calculated for each model. The clinical application value of the prediction models was determined through the decision curve analysis (DCA) by quantifying the net benefit to the patient under different threshold probabilities in the queue.

Development and validation of nomogram

To provide a visually quantitative tool to predict histologic subtype for TET patients, we develop a nomogram on the basis of the prediction model with the highest AUC value and clinical utility on training cohort. Calibration curve was plotted to assess the calibration of the nomogram by bootstrapping (1000 bootstrap resamples) based on internal (training cohort) and external (validation cohort) validity.

Results

Clinical and demographic characteristics

Totally 172 TET patients comprising of 87 LTET (n [type A] =6; n [type AB] =66; n [type B1] =15) and 85 HTET (n [type B2] =41; n [type B3] =23; n [type C] =21) were enrolled in this study. Clinical and demographic characteristics in the training and validation cohorts are summarized and compared in **Table 1**. Patient's sex and age were highly related with the discrimination of the two subtypes (p<0.05, respectively). There are no significant differences in symptom between the LTET and HTET groups according to the univariate analysis in either the training or validation cohorts (p>0.05, respectively), consistent with the report [26].

Feature selection and prediction model establishment

A total of 12 CT signs and 43 texture features were extracted from 172 TET patients' enhanced CT images, and the agreement between the two radiologists (readers 1, 2) was excellent for texture features (all ICCs >0.85, p<0.05). Thus, the mean measurement values of the two radiologists were used for further analysis.

The cross-correlation matrixes showed that there were multiple complex cross-correlations among these parameters (**Fig. 2**). For differentiating LTET from HTET, 4 independent prediction models were built separately on the basis of selected clinical, CT, texture parameters and their combination by LASSO regression in the training cohort (**Fig. 3 a-d**). The Pre-scores of each model for each patient were calculated using the following calculation formulas:

Pre-scores (Clinical model) = 0.83 - 0.20*sex - 0.01*age;

Pre-scores (CT model) = -0.16 - 0.01*short diameter + 0.49*boundary + 0.63*mediastinum fat line;

Pre-scores (TA model) = 3.01 - 0.04*meanValue - 0.62*SHAPE_Sphericity -0.03*NGLDM_Busyness;

Pre-scores (Combined model) = 1.67 + 0.39*boundary + 0.46*mediastinum fat line -0.03*meanValue - 0.03*NGLDM_Busyness.

HTET patients generally had higher Pre-scores for all prediction models than LTET patients in both the training and validation cohorts (p <0.05, respectively) (**Table 2**).

Prediction performance and Clinical utility of predictive models

The performance of these 4 models to discriminate LTET from HTET is shown in **Table 3**, **Fig. 4**. By comparing the models, the discrimination capacity of Clinical model, CT model, TA model and Combined model increased in turn, which indicated that the Combined model presented the optimal discrimination and best predictive accuracy with the highest AUC value and accuracy in both the training cohort (AUC [95% CI] = 0.88 [0.81-0.94], accuracy=79.2%) and the validation cohort (AUC [95% CI] = 0.94 [0.89–0.98] , accuracy=86.5%) (**Table 3**).

The DCAs also showed that the clinical application value of these 4 prediction models increased in turn, which indicated that the Combined model incorporating CT morphological features and texture

parameters was a most reliable clinical treatment tool for predicting histologic subtypes in TET patients when the threshold probability was between 0.02 and 0.91 (**Fig. 5**).

Development and validation of nomogram

According to the above results, we generated a nomogram based on the parameters of the Combined model for visualization (**Fig. 6**). The calibration curves of nomogram for the probability of HTET demonstrated a good agreement between prediction by nomogram and actual observation in two cohorts (p >0.05, respectively) (**Fig. 7**).

Discussion

In the present study, we developed 4 independent prediction models to differentiate the pathologic subtypes of TETs, and constructed a quantitative nomogram based on the model which held the highest efficiency and clinical utility. This nomogram was validated for the preoperative individualized prediction of the classification in TET patients.

In terms of clinical characteristics and CT signs, although the correlation between patient's gender, age and tumor invasiveness is still controversial [2; 4; 15], our study indicated that an older female TET patient with a bigger tumor size, a smoother boundary and a clearer mediastinum fat line indicates a lower probability that the tumor is malignant. In this study, tumor size, boundary and mediastinum fat line were significantly associated with the malignant grade of TETs. According to the general understanding, the larger the tumor, the more malignant it is [27]. However, the size in LTET was larger than that in HTET in both the training and validation cohorts (p values < 0.05, respectively). This may be related to the fact that the less aggressive the tumor is, the lighter clinical symptoms the patient has, which leads to a larger volume when it is found. The boundary and mediastinum fat line of tumor on CT images can reflect the invasiveness of the mass to a certain extent [28; 29]. There is usually a higher rate of tumor invasiveness by directly extending to adjacent structures including vessels, pericardium or lung, which is shown as a rough boundary and blurred or even disappeared fat line. The results of this study are basically consistent with previous researches.

In this study, the texture parameters of meanValue, sphericity and NGLDM_Busyness of LTET patients were higher than HTET ones. Meanwhile, the TA model composed of these 3 parameters held great individualized prediction for TET patients (AUCs = 0.82 [training cohort], 0.86 [validation cohort], respectively). MeanValue in histogram, which represent the average value of ROI, reflects the degree of texture regularity: the higher the value, the more regular the texture is, that is, the lower the heterogeneity is. Yasaka K et al. also found that the meanValue was a significant parameter for differentiating between HTET and LTET with AUC of 0.89 [21]. Sphericity is the shape features of tumors, and has been proven as the most significant affecting factor for discriminating histologic subtype in TET patients [30]. Busyness is a parameter of NGLDM, which measures the spatial frequency of changes in intensity between nearby voxels of different grey-levels. The role of busyness in TETs has not been reported before, but it has been used to assess the tissue heterogeneity in glioma and lung cancer [31–33]. Heterogeneity is a recognized

feature of tumors that considered to be positively correlated with the tumor malignancy, which is of great clinical significance for effective personalized therapies [34; 35]. Previous studies also demonstrated that thymic carcinoma, type B2 and B3 thymomas are generally more heterogeneous compared with type A, AB, B1 thymomas [36–38]. The results of this study are consistent with the conclusion of the above reports.

This study also explored whether the prediction performance based on texture analysis could be improved by combination with conventional CT diagnosis. The Combined model developed in present study was composed of the boundary and mediastinum fat line of CT signs and the meanValue and NGLDM_Busyness of texture parameters, and this model was most advantageous than did the use of either them alone. The accuracy of the Combined model was also superior. The results of this study confirm the hypothesis and indicate that the heterogeneity of tumor can be evaluated more comprehensively by combining with the macroscopic and internal characteristics of tumor. In addition, we generated a nomogram on the basis of the Combined model for facilitating clinical use, and recommend that male patients with a younger age, a smaller tumor size, a rougher boundary, a unclearer mediastinum fat line shown on preoperative enhanced CT images should have regular follow-ups, and the progression of the disease should be closely monitored in these TET patients. In addition, we suggest that patients with a higher-risk of TET, as screened by the nomogram, should be considered potential adjuvant therapy candidates to extend survival. The clinical application of this nomogram can reduce the cost of subsequent diagnosis, help develop more reasonable and effective treatment plans and prevent patients from having a poor prognosis.

However, the present study had several limitations although the results were encouraging. First, the sample selection was biased in this retrospective study, and a prospective study is required to confirm and validate the prediction nomogram. Second, the texture features extracted in this study were only based on enhanced CT images, but not the plain CT. However, previous study showed that there was no significant difference between radiomics features based on plain CT images and ones based on enhanced CT images for predicting risk categorization of TETs [30]. Third, the tumor, node, metastasis (TNM) [39] or Masaoka [40] staging systems for TETs were not used in this study. Further study will be needed to reveal the relationship with texture features and TNM or Masaoka staging systems.

Conclusions

A prediction nomogram incorporating both the CT morphological features and texture parameters was constructed and validated in our study, which was conveniently used to facilitate the preoperative individualized prediction of simplified histologic subtypes in TET patients, assisting in clinical treatment decision making and achieving precision treatment.

Abbreviations

3D

three-dimensional
AUC
the area under ROC curve
CI
confidence intervals
CT
computed tomography
DCA
decision curve analysis
GLCM
Gray-Level Co-occurrence Matrix
GLRLM
Gray-Level Run Length Matrix
GLZLM
Gray-Level Zone Length Matrix
HTET
high-risk TET
ICCs
intra- and interclass correlation coefficients
LASSO
least absolute shrinkage and selection operator
LTET
low-risk TET
MRI
magnetic resonance imaging
NGLDM
Neighboring Gray-Level Dependence Matrix
PACS
picture archiving and communication system
PET/CT
positron emission tomography-computed tomography
Pre-score
prediction score
ROC
receiver operating characteristic
ROI
region of interest
TA
texture analysis
TET

thymic epithelial tumor
TNM
tumor, node, metastasis
WHO
World Health Organization

Declarations

Ethics approval and consent to participate: Our Institutional Review Boards (Shanghai Proton and Heavy Ion Center and Fudan University Shanghai Cancer Center Medical Ethics Committees) approved this retrospective study and waived the need for informed consent from patients.

Consent for publication: All authors have read and approved the content and agree to submit for consideration for publication in the journal.

Availability of data and materials: Yes.

Competing interests: The authors declare that they have no competing interests.

Funding: Our research did not receive specific funding.

Authors' contributions: Ren CY designed the research; LI ML and Zhang YY reviewed the CT images and extracted the texture features; Ren CY performed the statistical analysis and drafted the manuscript; Zhang SJ participated in its design and coordination, helped to draft the manuscript. All authors read and approved the final manuscript.

Acknowledgements: All the authors have contributed significantly and have approved the manuscript.

References

1 Marom EM (2013) Advances in Thymoma Imaging. Journal of Thoracic Imaging 28:69-83

2 Kondo K, Yoshizawa K, Tsuyuguchi M et al (2004) WHO histologic classification is a prognostic indicator in thymoma. Ann Thorac Surg 77:1183-1188

3 Hosaka Y, Tsuchida M, Toyabe S, Umezu H, Eimoto T, Hayashi JI (2010) Masaoka Stage and Histologic Grade Predict Prognosis in Patients With Thymic Carcinoma. Annals of Thoracic Surgery 89:912-917

4 Travis WD, Brambilla, E., Burke, A.P., Marx, A., Nicholson, A. G. (2015) WHO Classification of Tumours of the Lung, Pleura, Thymus and Heart. Fourth edition. IARC Press ;

5 Okumura M, Ohta M, Tateyama H et al (2002) The World Health Organization histologic classification system reflects the oncologic behavior of thymoma: a clinical study of 273 patients. Cancer

94:624-632

6 Inoue A, Tomiyama N, Tatsumi M et al (2009) (18)F-FDG PET for the evaluation of thymic epithelial tumors: Correlation with the World Health Organization classification in addition to dual-time-point imaging. Eur J Nucl Med Mol Imaging 36:1219-1225

7 Lattanzio R, La Sorda R, Facciolo F et al (2014) Thymic epithelial tumors express vascular endothelial growth factors and their receptors as potential targets of antiangiogenic therapy: a tissue micro array-based multicenter study. Lung Cancer 85:191-196

8 Chen G, Marx A, Chen WH et al (2002) New WHO histologic classification predicts prognosis of thymic epithelial tumors: a clinicopathologic study of 200 thymoma cases from China. Cancer 95:420-429

9 Terzi A, Bertolaccini L, Rizzardi G et al (2011) Usefulness of 18-F FDG PET/CT in the pre-treatment evaluation of thymic epithelial neoplasms. Lung Cancer 74:239-243

10 Saif MW, Tzannou I, Makrilia N, Syrigos K (2010) Role and cost effectiveness of PET/CT in management of patients with cancer. Yale J Biol Med 83:53-65

11 Priola AM, Priola SM, Giraudo MT et al (2016) Diffusion-weighted magnetic resonance imaging of thymoma: ability of the Apparent Diffusion Coefficient in predicting the World Health Organization (WHO) classification and the Masaoka-Koga staging system and its prognostic significance on disease-free survival. Eur Radiol 26:2126-2138

12 Jeong YJ, Lee KS, Kim J, Shim YM, Han JH, Kwon OJ (2004) Does CT of thymic epithelial tumors enable us to differentiate histologic subtypes and predict prognosis? American Journal of Roentgenology 183:283-289

13 Moon JW, Lee KS, Shin MH et al (2015) Thymic epithelial tumors: prognostic determinants among clinical, histopathologic, and computed tomography findings. Ann Thorac Surg 99:462-470

14 Choe J, Lee SM, Lim S et al (2017) Doubling time of thymic epithelial tumours on CT: correlation with histological subtype. Eur Radiol 27:4030-4036

15 Han X, Gao W, Chen Y et al (2019) Relationship Between Computed Tomography Imaging Features and Clinical Characteristics, Masaoka-Koga Stages, and World Health Organization Histological Classifications of Thymoma. Front Oncol 9:1041

16 Davnall F, Yip CS, Ljungqvist G et al (2012) Assessment of tumor heterogeneity: an emerging imaging tool for clinical practice? Insights Imaging 3:573-589

17 Ganeshan B, Miles KA (2013) Quantifying tumour heterogeneity with CT. Cancer Imaging 13:140-149

18 Lubner MG, Smith AD, Sandrasegaran K, Sahani DV, Pickhardt PJ (2017) CT Texture Analysis: Definitions, Applications, Biologic Correlates, and Challenges. Radiographics 37:1483-1503

19 Fujita A, Buch K, Li B, Kawashima Y, Qureshi MM, Sakai O (2016) Difference Between HPV-Positive and HPV-Negative Non-Oropharyngeal Head and Neck Cancer: Texture Analysis Features on CT. Journal of Computer Assisted Tomography 40:43-47

20 Liu LH, Liu YH, Xu L et al (2017) Application of texture analysis based on apparent diffusion coefficient maps in discriminating different stages of rectal cancer. Journal of Magnetic Resonance Imaging 45:1798-1808

21 Yasaka K, Akai H, Nojima M et al (2017) Quantitative computed tomography texture analysis for estimating histological subtypes of thymic epithelial tumors. European Journal of Radiology 92:84-92

22 Iannarelli A, Sacconi B, Tomei F et al (2018) Analysis of CT features and quantitative texture analysis in patients with thymic tumors: correlation with grading and staging. Radiol Med 123:345-350

23 Orlhac F, Nioche C, Soussan M, Buvat I (2016) Understanding changes in tumor textural indices in PET: a comparison between visual assessment and index values in simulated and patient data. Journal of Nuclear Medicine Official Publication Society of Nuclear Medicine 58

24 Tibshirani R (1996) Regression shrinkage and selection via the Lasso. Journal of the Royal Statistical Society Series B-Methodological 58:267-288

25 Sauerbrei W, Royston P, Binder H (2007) Selection of important variables and determination of functional form for continuous predictors in multivariable model building. Stat Med 26:5512-5528

26 Strobel P, Bauer A, Puppe B et al (2004) Tumor recurrence and survival in patients treated for thymomas and thymic squamous cell carcinomas: a retrospective analysis. J Clin Oncol 22:1501-1509

27 Feng XL, Lei XB, Dong WT et al (2018) Incidence and clinical variable inter-relationships of thymic epithelial tumors in northwest China. J Thorac Dis 10:6794-6802

28 Tomiyama N, Johkoh T, Mihara N et al (2002) Using the World Health Organization classification of thymic epithelial neoplasms to describe CT findings. American Journal of Roentgenology 179

29 Hu YC, Wu L, Yan LF et al (2014) Predicting subtypes of thymic epithelial tumors using CT: new perspective based on a comprehensive analysis of 216 patients. Sci Rep 4:6984

30 Wang X, Sun W, Liang H, Mao X, Lu Z (2019) Radiomics Signatures of Computed Tomography Imaging for Predicting Risk Categorization and Clinical Stage of Thymomas. Biomed Res Int 2019:3616852

31 Raja R, Sinha N, Saini J, Mahadevan A, Rao KN, Swaminathan A (2016) Assessment of tissue heterogeneity using diffusion tensor and diffusion kurtosis imaging for grading gliomas. Neuroradiology 58:1217-1231

32 Chen S, Harmon S, Perk T et al (2019) Using neighborhood gray tone difference matrix texture features on dual time point PET/CT images to differentiate malignant from benign FDG-avid solitary pulmonary nodules. Cancer Imaging 19:56

33 Ferreira-Junior JR, Koenigkam-Santos M, Magalhaes Tenorio AP et al (2020) CT-based radiomics for prediction of histologic subtype and metastatic disease in primary malignant lung neoplasms. Int J Comput Assist Radiol Surg 15:163-172

34 Ganeshan B, Panayiotou E, Burnand K, Dizdarevic S, Miles K (2012) Tumour heterogeneity in non-small cell lung carcinoma assessed by CT texture analysis: a potential marker of survival. European Radiology 22:796-802

35 Dagogo-Jack I, Shaw AT (2018) Tumour heterogeneity and resistance to cancer therapies. Nat Rev Clin Oncol 15:81-94

36 Moran CA, Suster S (2000) On the histologic heterogeneity of thymic epithelial neoplasms - Impact of sampling in subtyping and classification of thymomas. American Journal of Clinical Pathology 114:760-766

37 Cheney RT (2010) The Biologic Spectrum of Thymic Epithelial Neoplasms: Current Status and Future Prospects. Journal of the National Comprehensive Cancer Network 8:1322-1328

38 Wheler J, Hong D, Swisher SG et al (2013) Thymoma Patients Treated in a Phase I Clinic at MD Anderson Cancer Center: Responses to mTOR Inhibitors and Molecular Analyses. Oncotarget 4:890-898

39 Detterbeck FC, Stratton K, Giroux D et al (2014) The IASLC/ITMIG Thymic Epithelial Tumors Staging Project: Proposal for an Evidence-Based Stage Classification System for the Forthcoming (8th) Edition of the TNM Classification of Malignant Tumors. Journal of Thoracic Oncology 9:S65-S72

40 Masaoka A, Monden Y, Nakahara K, Tanioka T (1981) Follow-up-Study of Thymomas with Special Reference to Their Clinical Stages. Cancer 48:2485-2492

Tables

Table 1 Clinical and demographic characteristics of TET patients

Characteristics	Training cohort		*p*-value	Validation cohort		*p*-value
	LTET (n=61)	HTET (n=59)		LTET (n=26)	HTET (n=26)	
Sex (%)			0.04			0.03
Male	28 (45.90%)	38 (64.41%)		11 (42.31%)	18 (69.23%)	
Female	33 (54.10%)	21 (35.59%)		15 (57.69%)	8 (30.77%)	
Age (mean ± SD, years)	56.44±9.48	51.76±12.08	0.02	56.50±8.30	54.53±11.02	0.04
Symptom (%)			0.28			0.57
+	25 (40.98%)	30 (50.85%)		12 (46.15%)	16 (61.54%)	
-	36 (59.02%)	29 (49.15%)		14 (53.85%)	10 (38.46%)	

Note: LTET, low-risk thymic epithelial tumor; HTET, high-risk TET; SD, standard deviation; *p*-values were the results of univariable association analyses of each characteristic

Table 2 Pre-scores of prediction models and their compositions of TET patients in the training cohort

	LTET (n=61)	HTET (n=59)	*p*-value
Short diameter (mean ± SD, mm)	35.48±16.44	29.85±12.52	0.04
Boundary (%)			0.00
Smooth	53 (86.89%)	30 (50.85%)	
Rough	8 (13.11%)	29 (49.15%)	
Mediastinum fat line (%)			0.00
clear	45 (73.77%)	20 (33.90%)	
unclear	16 (26.23%)	39 (66.10%)	
MeanValue	68.63 (56.52, 78.55) *	48.84 (40.82, 58.18) *	0.00
SHAPE_Sphericity	0.95 (0.93, 0.97) *	0.93 (0.90, 0.96) *	0.01
NGLDM_Busyness	1.13 (0.36, 3.64) *	0.91 (0.43, 1.63) *	0.01
Pre-scores (Clinical model)	-0.11 (-0.23, 0.06) *	-0.01 (-0.11, 0.13) *	0.00
Pre-scores (CT model)	-0.37 (-0.50, -0.22) *	0.29 (-0.33, 0.63) *	0.00
Pre-scores (TA model)	-0.53 (-0.85, 0.02) *	0.32 (-0.01, 0.76) *	0.00
Pre-scores (Combined model)	-0.53 (-0.99, -0.05) *	0.52 (0.03, 0.84) *	0.00

Note: NGLDM, Neighboring Gray-Level Dependence Matrix; CT, computed tomography; TA, texture analysis; *Values refer to median (interquartile range (IQR)).

Table 3 Prediction performance of the 4 prediction models

Training cohort	AUC	95% CI	Sensitivity (%)	Specificity (%)	Accuracy (%)
Clinical model	0.66	0.56-0.75	81.4	45.9	59.2
CT model	0.79	0.70-0.87	66.1	83.6	71.7
TA model	0.82	0.74-0.89	94.9	60.7	75.0
Combined model	0.88	0.81-0.94	93.2	67.2	79.2
Validation cohort	**AUC**	**95% CI**	**Sensitivity (%)**	**Specificity (%)**	**Accuracy (%)**
Clinical model	0.64	0.49-0.79	73.1	61.5	57.7
CT model	0.82	0.70-0.93	96.2	53.8	69.2
TA model	0.86	0.76-0.96	88.5	73.1	75.0
Combined model	0.94	0.89-0.98	96.2	80.8	86.5

Note: AUC, area under the receiver operating curve; 95% CI: 95% confidence interval.

Figures

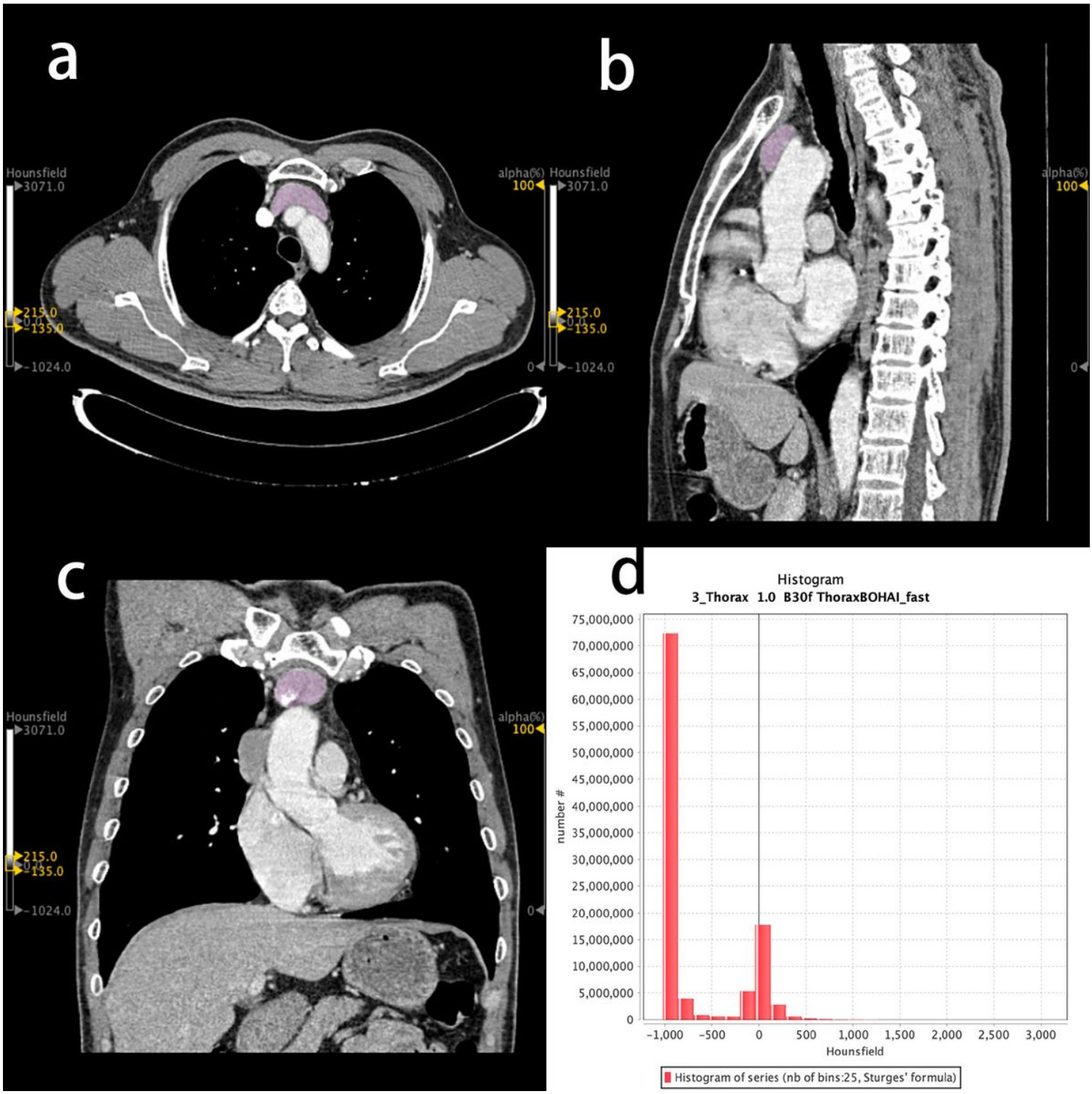

Figure 1

Chest enhanced CT images of a 53-years-old man with type B1 thymic epithelial tumor (low-risk TET). Texture features are extracted from the primary tumor area (purple overlay). (a) transverse section; (b) median sagittal section; (c) coronal section; (d) histogram.

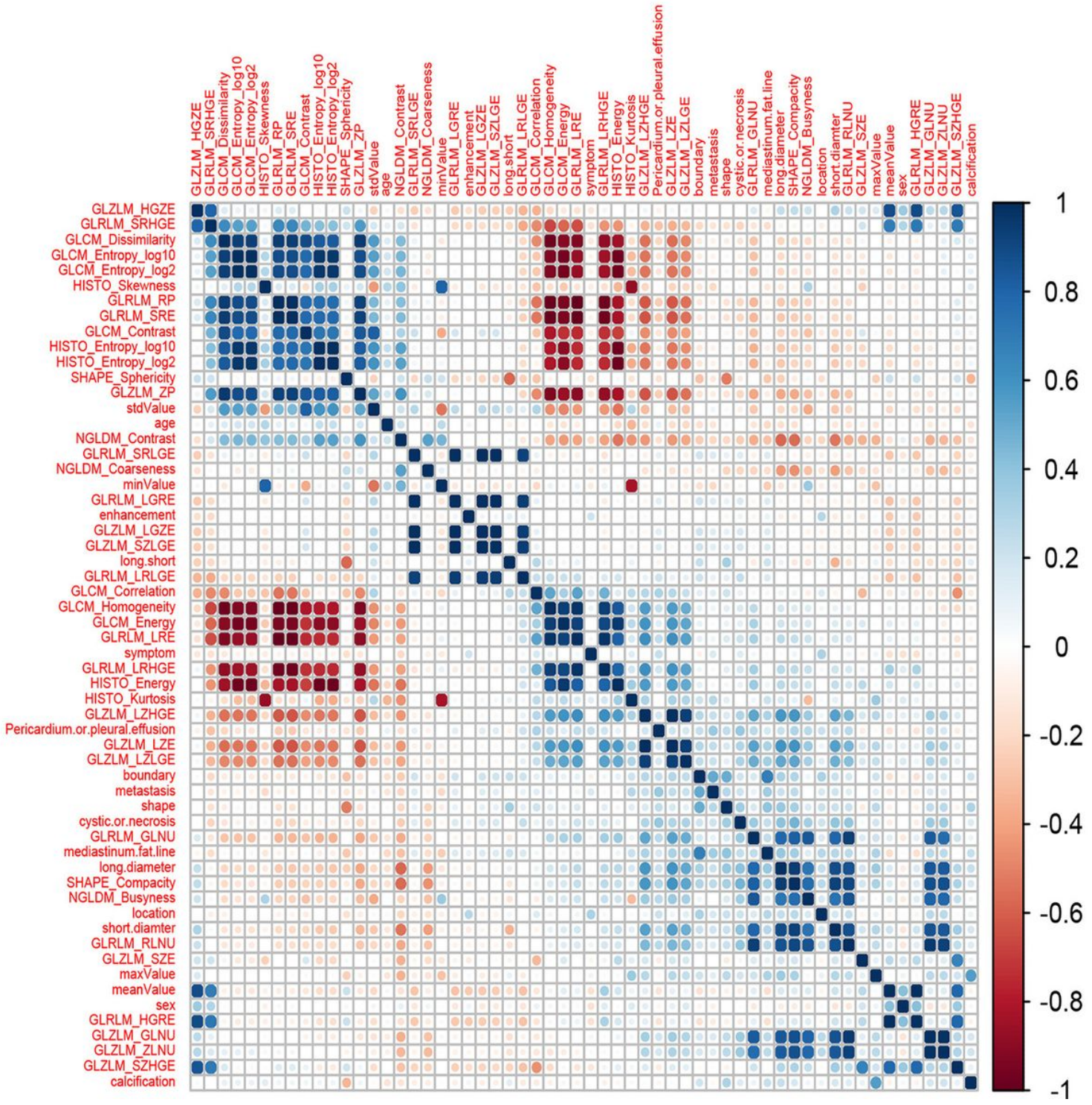

Figure 2

The cross-correlation matrix for covariates. Blue represents positive correlation and red represents negative correlation. The depth of color indicates the intensity of the correlation between covariates. The darker the color, the higher the correlation is.

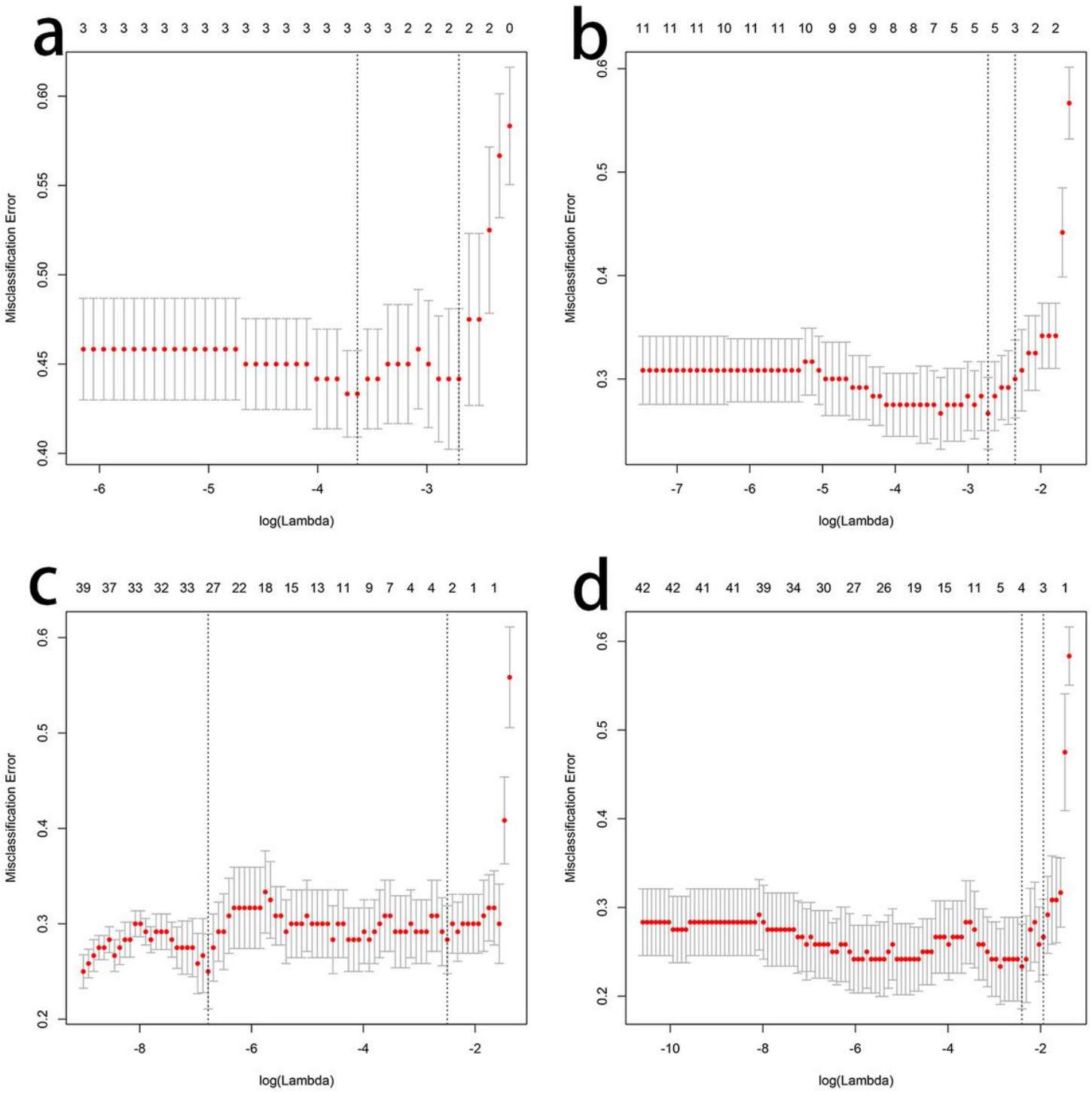

Figure 3

Features selection for prediction models by LASSO regression. Tuning parameter (λ) selection used 10-folds cross-validation. The X-axis shows log (λ), and the Y-axis shows the model misclassification rate. The 2, 3, 3,4 features with non-zero coefficients are indicated with the optimal λ value of 0.07, 0.10, 0.08, 0.10 for Clinical model (a), CT model (b), TA model (c), Combined model (d), respectively.

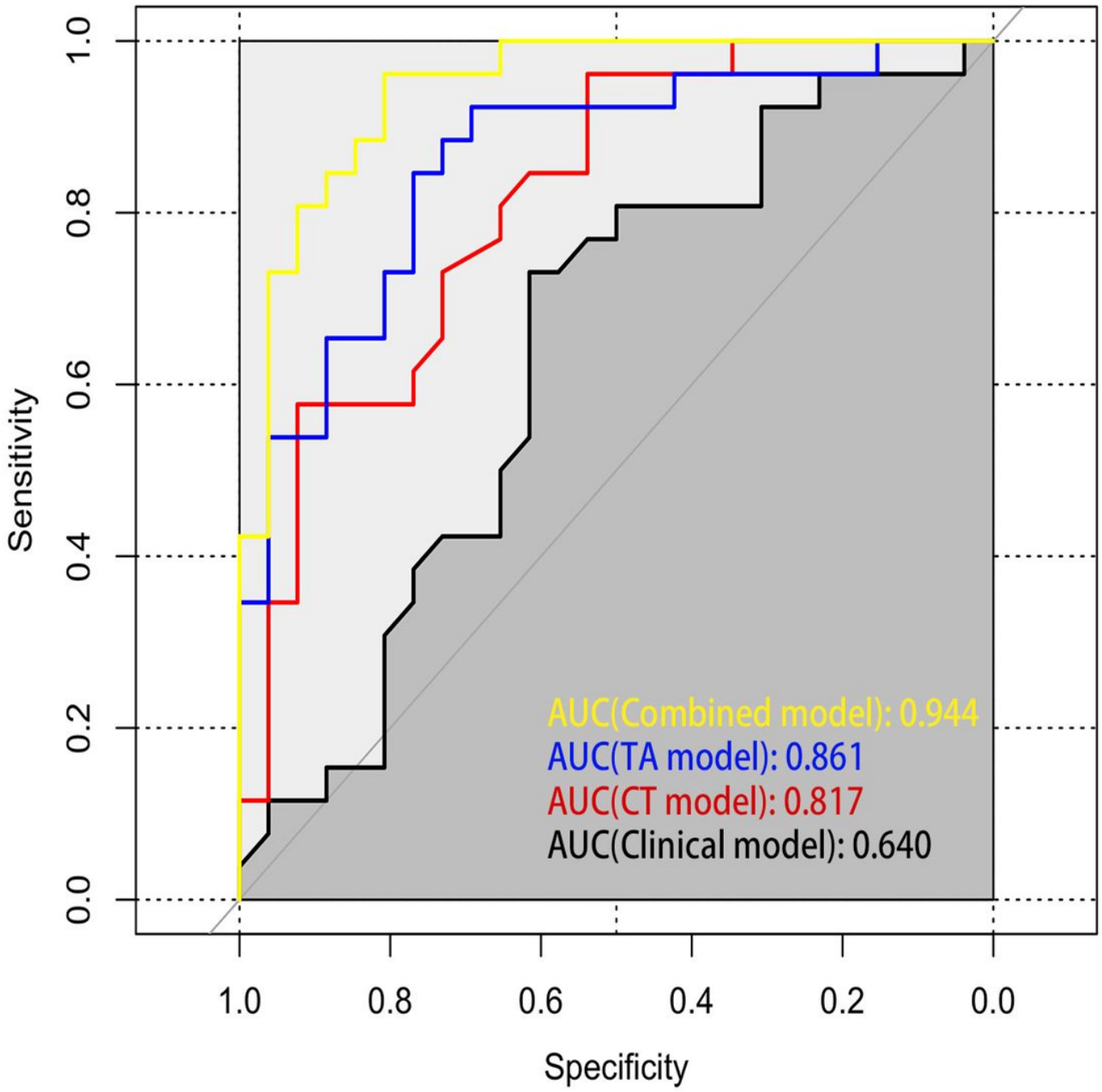

Figure 4

ROC curve analysis of the prediction models in the validation cohort.

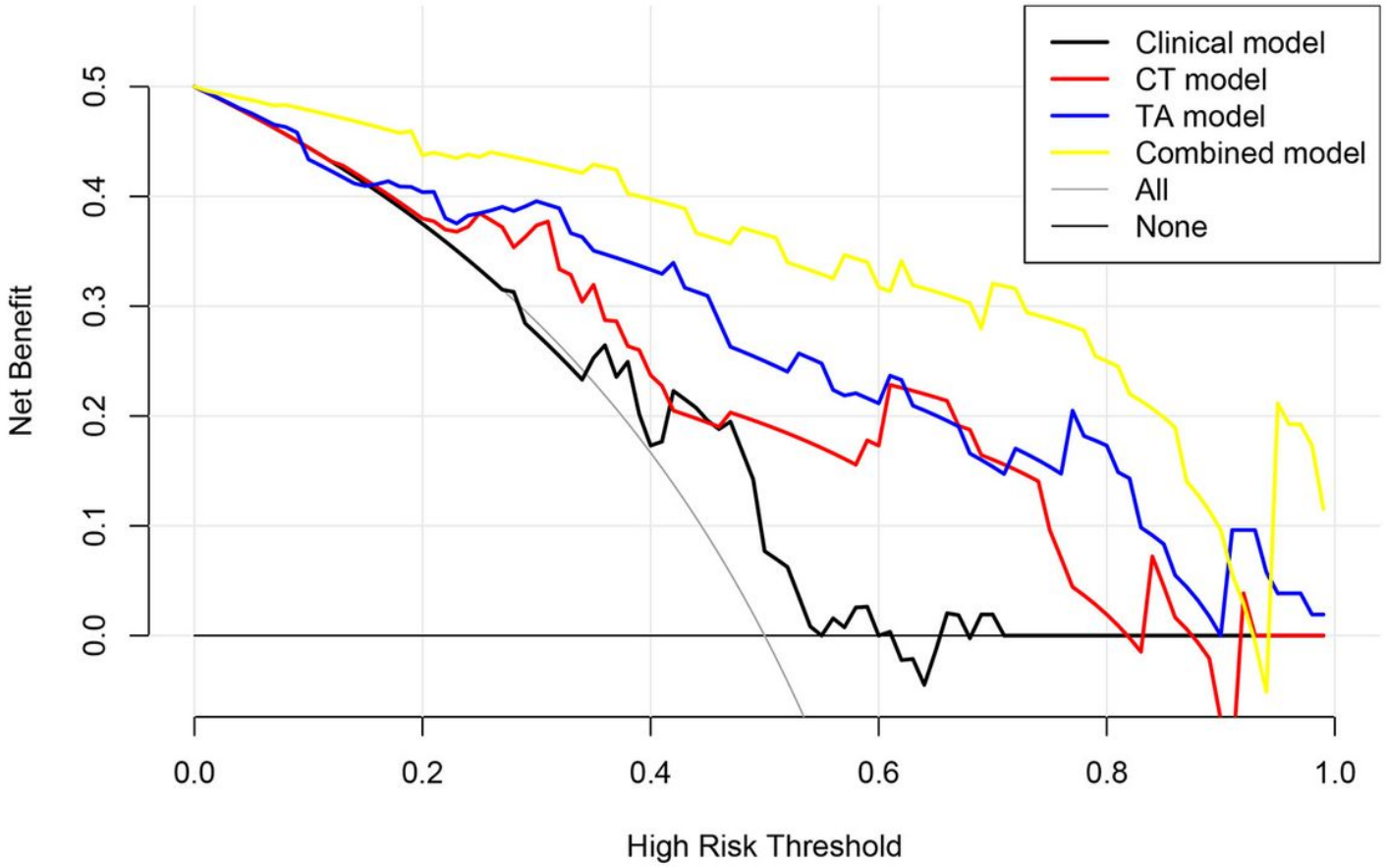

Figure 5

DCA for the prediction models. The X-axis represents the threshold probability. The Y-axis represents the net benefit. The grey and black thin lines represent the hypothesis that all TET patients are high-risk or low-risk, respectively. The higher curve at any given threshold probability is the optimal prediction to maximize net benefit.

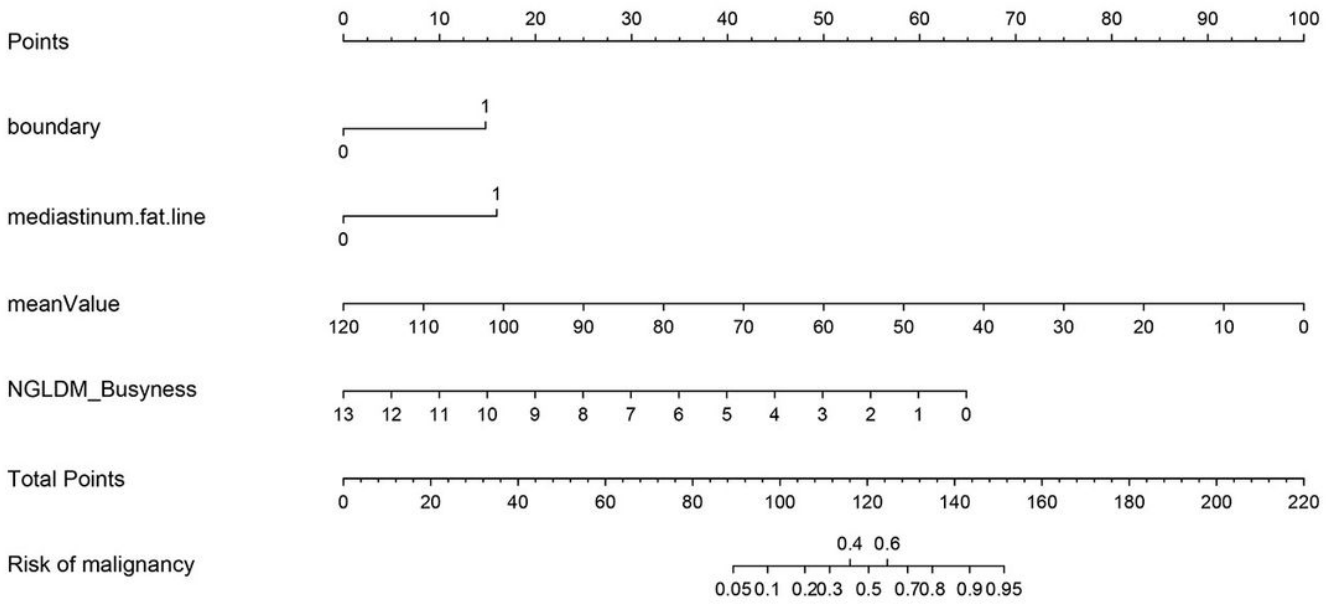

Figure 6

Developed prediction nomogram in the training cohort. The probability of each predictor can be converted into scores according to the first scale “Points” at the top of the nomogram. After adding up the corresponding prediction probability at the bottom of the nomogram is the malignancy of the tumor.

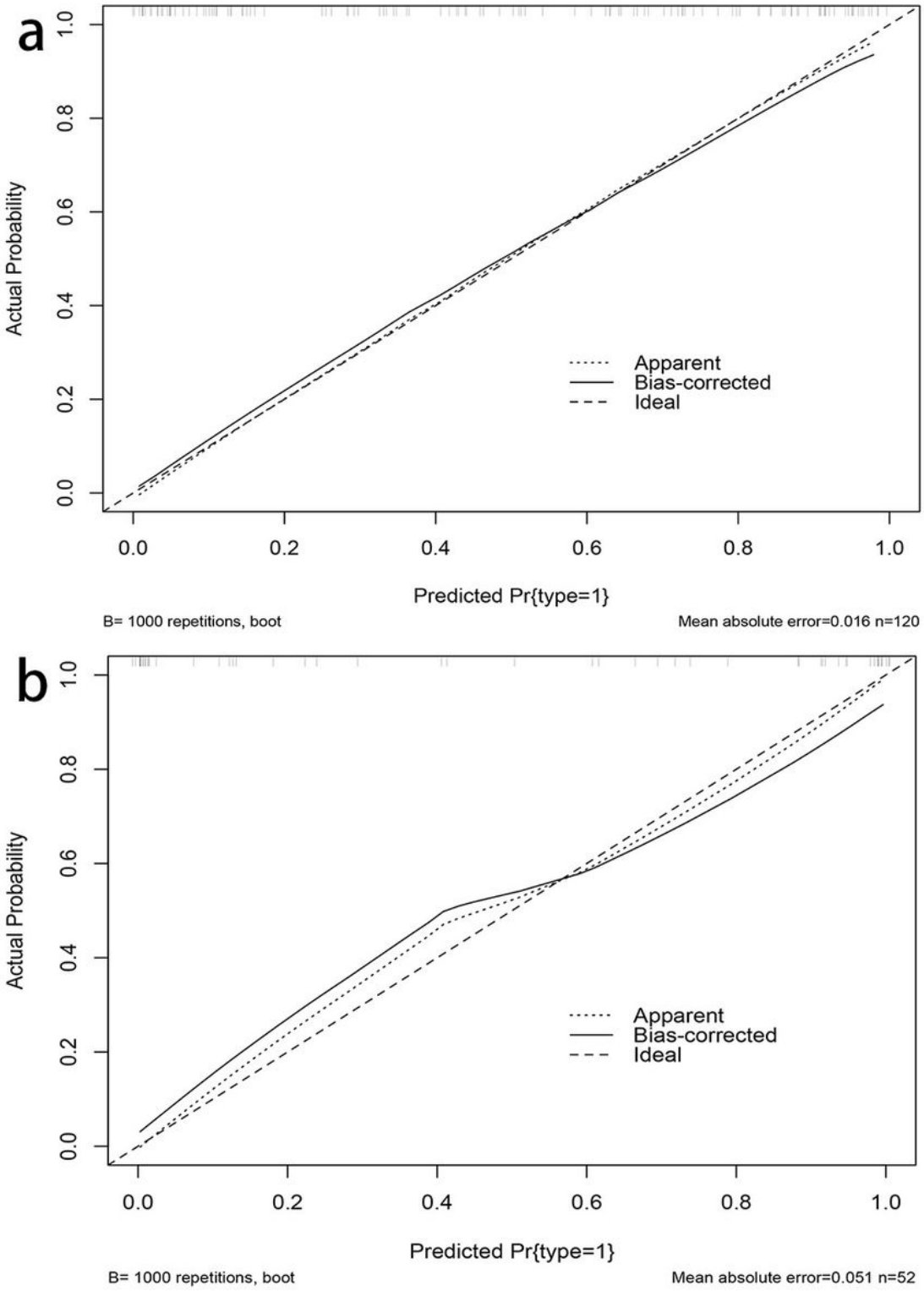

Figure 7

Calibration curves of the nomogram in training (a) and validation (b) cohorts. The X-axis represents the predicted malignancy probability estimated by the nomogram whereas the Y-axis represents the actual observed rates of HTET. The solid line represents the ideal reference line that predicted TET malignant corresponds to the actual outcome, the short-dashed line represents the apparent prediction of nomogram, and the long-dashed line represents the ideal estimation.

Supplementary Files

This is a list of supplementary files associated with this preprint. Click to download.

- Appendices.doc